FERMILAB-PUB-08-617-AD

Magnetron-Driven Microtron-Injector of a Terahertz Free Electron Laser*

Grigory M. Kazakevich**
Budker Institute of Nuclear Physics RAS, (BINP), Academician Lavrentyev 11, Novosibirsk, 630090, Russia and Fermi National Accelerator Laboratory, P.O. Box 500, Batavia, IL 60510, U.S.A.

Viatcheslav M. Pavlov
Budker Institute of Nuclear Physics RAS, (BINP), Academician Lavrentyev 11, Novosibirsk, 630090, Russia

Young Uk Jeong and Byung Cheol Lee
Korea Atomic Energy Research Institute, (KAERI), P. O. Box 105, Yusong, Taejon, 305-600, South Korea

A magnetron-driven microtron-injector has been developed for a terahertz Free Electron Laser (FEL). An internal injection system was chosen for the microtron to achieve a compact and inexpensive design. The system provides acceleration of electrons with low emittance and energy spread that is highly important for the FEL. However the intrapulse instabilities of the accelerated current and the bunch repetition rate inherent to the injection system make problems for the FEL operation. Simulations of the beam dynamics and the transient process allow one to compute the load characteristic of the accelerating cavity and the time-dependent accelerated current. The simulation techniques also allow one to calculate time-dependent deviations of the magnetron frequency in the coupled system of the accelerating and magnetron cavities, as well as deviations in the bunch repetition rate. The computations validate proposed concepts for increasing the intrapulse current stability with appropriate time-dependent variation of the magnetron power and decreasing the bunch repetition rate instability through a simple microwave scheme utilizing the microtron accelerating cavity concurrently as an external stabilizing resonator for the magnetron. The realized concepts and optimization of the microtron regimes using the simulated phase motion of the accelerated bunch provides stable operation of the terahertz FEL, tunable in the range of 1-3 THz with extracted macro-pulse power up to 50 Watts at the macro-pulse energy of ~ 0.2 mJ.

PACS codes: 41.60.Cr; 07.57.Hm; 29.20.-C

Introduction

A compact high-current microtron-injector driven by MI-456A magnetron [1] has been developed for a laboratory-size terahertz FEL, tunable in the range of 1-3 THz [2]. The 12-orbit microtron employing the I-type internal injection, [3], provides stable operation of the FEL. Parameters of the magnetron and parameters of the microtron optimal for the FEL operation are shown in Tables I and II, respectively.

Table I. The magnetron main parameters

Magnetron operating frequency	2800±5 MHz
Magnetron cavity coupling coefficient	≅10
Magnetron cavity wall Q-factor	~1500
External waveguide conductance	$2.363\cdot10^{-3}$ Ohm^{-1}
Magnetron pulse power	2.5 MW
Magnetron macro-pulse current width	7.3 μs
Magnetron duty factor	≤0.002

Table II. Main parameters of the microtron

Microtron cavity eigen frequency	2800 MHz
Microtron cavity coupling coefficient	5.4
Microtron cavity wall Q-factor	9800
External waveguide conductance	$1\cdot10^{-5}$ Ohm^{-1}
Shunt impedance	1.08 MOhm
Electron beam energy increment per turn	0.544 MeV
Microtron permanent magnetic field	0.1065 T
12th orbit accelerated macro-pulse current	45-50 mA
Accelerated macro-pulse current width	6 μs

Precise motion of the accelerating cavity inside the microtron magnetic system allows to extract the accelerated electrons from various orbits; this varies kinetic energy of the beam approximately from 4.4 MeV to 6.5 MeV and provides generation of the terahertz FEL in wide range. Note that at lower energy the microtron at optimal regime accelerates higher current; e.g. the 8th orbit accelerated macro-pulse current is ≈ 70 mA.

The regime of the microtron requires the macro-pulse emission current of ~1 A. Such a value of the emission current causes noticeable pulsed overheating of the cathode surface because of the back-streaming electrons. The phenomenon in the microtron with internal injection causes

*This work was supported in frames of scientific collaboration between the BINP and the KAERI and by Fermi Research Alliance, LLC under Contract No. DE-AC02-07CH11359 with the US Department of Energy.
**e-mail: gkazakevitch@yahoo.com

increments of the emission current during the macro pulse and as a result, incremental beam loading in the accelerating cavity, [4]. This causes a drop of the accelerating field resulting in a decrease of the accelerated current at a constant power feeding the accelerating cavity.

Based on 2D beam tracking in the microtron median plane, we studied this phenomenon using a numerical simulation of the transient state of the accelerating cavity loaded by the electron beam [5]. The simulation shows a significant drop in the accelerated current during the macro pulse for measured increments of the emission current. To keep the accelerated current constant during the macro-pulse we tuned the modulator charging line to provide linear enhancement of the magnetron current. In this case, as follows from simulation and measurements, the accelerated current has a flat top providing intrapulse stability of the beam current suitable for FEL operation. However, the incremental magnetron current deteriorates the intrapulse frequency stability of the magnetron auto-generator because of the frequency pushing. Correspondingly the bunch repetition rate stability becomes worse, leading to a drop of the lasing energy.

A simple microwave scheme based on the frequency pulling in the magnetron and utilizing the reflected wave from the accelerating cavity was developed to stabilize the magnetron frequency and the bunch repetition rate. The scheme was numerically simulated using the transient state of the system including the magnetron resonance system and the accelerating cavity coupled through a ferrite insulator. The simulation and the measurements are in good agreement and showed that the developed microwave scheme effectively decreases the frequency instability of the magnetron auto-generator. This reduces the bunch repetition rate instability during the macro pulse to a level that is acceptable for terahertz FEL operation. Simulation of the beam dynamics and consideration of the transient state in the accelerating cavity demonstrates the equilibrium phase variation during the transient process that deteriorates FEL operation. The performed calculation shows how to optimize the microtron regimes minimizing the variation. A FEL macro-pulse energy ≈ 0.2 mJ was obtained employing the optimization.

The concepts of the intrapulse stabilizations realized in the magnetron-based microtron driving the terahertz FEL at optimized regimes, 2D tracking, simulation of the stabilizations and measured results including data obtained at the FEL operation are presented and discussed in this article.

Simulation of the Plane Tracking in the Microtron with Internal Injection

Simulation of the tracking in the microtron was done for TM_{010} mode of the accelerating field in a cylindrical cavity having radius R and length L with I-type internal injection.

Considering the plane motion of the electrons, one assumes that the n-th particle having a macro particle charge of q enters into the cavity at the time of t_{0n}. At the time of t, the particle is located at the point with coordinates of $y_n = 0$, $x_n(t_{0n},t)$ and $z_n(t_{0n},t)$ having velocity of $\vec{v}_n(t_{0n},t)$.

The coordinates $x_n(t_{0n},t)$ and velocities $v_{zn}(t_{0n},t)$ have been calculated for a given amplitude of the cavity complex voltage $V_C = \left|\tilde{V}_C\right|$, in 2D code considering the motion in the median plane ($\vec{z}^{\,0}, \vec{x}^{\,0}$), and using the Lorentz-force equation:

$$\frac{d\vec{p}}{dt} = e \cdot \left\{\vec{E}(\vec{r},t) + \left[\vec{v} \times \vec{B}\right]\right\}. \qquad (1)$$

Here $\vec{E}(\vec{r},t)$ is the electric field acting on the electron at the point with coordinate $\vec{r}$ and the time t, $\vec{v}$ is the velocity of the electron at this point at time t, and $\vec{B}$ is the magnetic field acting on the electron ($\vec{B}$ includes the RF component in the accelerating cavity and the permanent microtron field) .

Unlike the ordinary tracking simulations described in a number of articles, [6, 7], we compute concurrently the load characteristic of the accelerating cavity, $\tilde{I}_C(V_C)$, where $\tilde{I}_C$ is the cavity loading current. This allows one to compute the accelerated current in the time domain considering the loading current effect. Moreover this allows one to compute frequency and phase deviation of the accelerated bunches that are important for the FEL injector.

Thus simulating the tracking, we determine the current density of n-th particle at time t at the point (x, y, z) which is equal to:

$$\begin{aligned}\vec{j}_n(x,y,z,t_{0n},t) = q \cdot \vec{v}_n(t_{0n},t) \cdot \delta(y) \times \\ \delta[x - x_n(t_{0n},t)] \cdot \delta[z - z_n(t_{0n},t)].\end{aligned} \qquad (2)$$

Here $t_{0n} = n \cdot \frac{T}{N}$, $n = 0,1,\ldots,N-1$, N is number of the particles, T is period of oscillations in the cavity, and

$$q = \begin{cases} \dfrac{I_{0C} \cdot T}{N} & \textit{for existent particles}, \\ 0 & \textit{for nonexistent particles}, \end{cases}$$

where I_{0C} is maximum of the cathode emission current.

The current density $\vec{j}_n$ is nonzero only inside the cavity. The first harmonic of the current density is equal to:

$$\tilde{\vec{I}}_1(\vec{r}) = \sum_{n=0}^{N-1}\left[\frac{2}{T} \cdot \int_{t_{0n}}^{t_{0n}+T} dt \left\{e^{-i\cdot\omega t} \cdot \vec{j}_n(x,y,z,t_{0n},t)\right\}\right]. \qquad (3)$$

Then the loading current $\tilde{I}_C$ correspondingly to [8] is:

$$\tilde{I}_C = i_C(t) \cdot \frac{1}{M} \cdot \int_v \tilde{\vec{I}}_1(\vec{r}) \cdot \vec{e}(\vec{r})\, dV, \qquad (4)$$

where $i_C(t)$ is the normalized dimensionless time-dependent slowly varying emission current, M is used for normalization:

$$M = \int_{-L/2}^{L/2} e_z(\vec{r}_\perp = 0, z) \cdot \exp\left(-i\omega_0 \cdot \frac{z}{v_0}\right) dz,$$

$\vec{e}(\vec{r})$ is a distribution of normalized electric field in the cavity, and v_0 is the average velocity of the electron ($v_0 \cong c$).

For the TM_{010}-mode in a cylindrical cavity, the distribution of the normalized electric field is expressed as:

$$\vec{e}(\vec{r}) = \vec{z}^{\,0} \cdot \left\langle -\sqrt{\frac{1}{\pi L}} \cdot \frac{1}{R} \cdot \frac{1}{J_1(\chi_{01})} \cdot J_0\left(\frac{\chi_{01} \cdot r}{R}\right) \right\rangle,$$

where J_0 and J_1 are the first kind Bessel functions, and $\chi_{01} = 2.405$ is the first zero of the Bessel function.

The loading current $\widetilde{I}_C$ one calculates as:

$$\widetilde{I}_C = \frac{2I_{0C} \cdot i_C(t)}{TTF \cdot L \cdot k_0} \cdot \frac{1}{N} \cdot \sum_{n=0}^{N-1} |w_n| \cdot \exp(-i\psi_n). \qquad (5)$$

Here $TTF = \dfrac{\sin(k_0 L/2)}{(k_0 L/2)}$ is the transit-time factor,

$$k_0 = \frac{2\pi}{\lambda_0} = \frac{\omega_0}{c}, |w_n| = \sqrt{w_{Cn}^2 + w_{Sn}^2}, \psi_n = \arctan\frac{w_{Sn}}{w_{Cn}}.$$

The functions w_{Cn} and w_{Sn} used in the loading current expression (5) are equal to:

$$w_{Cn} = \int_{t_{0n}}^{t_{0n}+t} v_{zn}(t_{0n}, t) \cdot J_0(k_0 \cdot x_n(t_{0n}, t)) \cdot \cos(\omega t)\, dt,$$

$$w_{Sn} = -\int_{t_{0n}}^{t_{0n}+t} v_{zn}(t_{0n}, t) \cdot J_0(k_0 \cdot x_n(t_{0n}, t)) \cdot \sin(\omega t)\, dt.$$

The following dimensionless variables have been used for tracking: $\varphi = \omega t$, $Z = k_0 z$, $X = k_0 x$, $L_0 = k_0 \cdot L$, $\vec{P} = \vec{p}/mc = \vec{\beta}\gamma$,

$$\Omega = \frac{\Omega_0}{\omega_0} = \frac{e \cdot B}{mck_0} = \frac{\lambda_0\ [\mathrm{m}]}{2\pi} \cdot \frac{300 \cdot B\ [\mathrm{T}]}{mc^2\,[\mathrm{MeV}]},$$

$$E = \frac{e \cdot E_0}{mc^2 k_0} = \frac{V_C\ [\mathrm{MV}]}{mc^2\,[\mathrm{MeV}]} \cdot \frac{1}{L[m] \cdot TTF}.$$

In terms of these variables, the motion of the n-th electron, and the current terms w_{Cn} and w_{Sn} are described by the following equation set (6) with the initial conditions for the n-th particle (7). Equations 5 and 6 in (6) for the current terms w_{Cn} and w_{Sn} are integrated inside the cavity only for $0 < Z_n(\varphi_n) < L_0$.

The equations were integrated up to the last (12-th) orbit for several cavity voltages V_C and for optimum value of the microtron magnetic field $B =$ 0.1065 T. The field corresponds to the electron beam energy increment per turn at the magnetron frequency of 2.8 GHz. The electrons hitting the cavity walls (inside or outside of the cavity) were omitted in the tracking.

$$\begin{cases} \dfrac{dP_{zn}}{d\varphi_n} = \dfrac{P_{xn}}{\gamma_n} \cdot \left[-\Omega - E \cdot J_1(X_n) \cdot \sin\varphi_n\right] + \\ \qquad E \cdot J_0(X_n) \cdot \cos\varphi_n \\ \dfrac{dP_{xn}}{d\varphi_n} = -\dfrac{P_{zn}}{\gamma_n} \cdot \left[-\Omega - E \cdot J_1(X_n) \cdot \sin\varphi_n\right] \\ \dfrac{dZ_n}{d\varphi_n} = \dfrac{P_{zn}}{\gamma_n} \\ \dfrac{dX_n}{d\varphi_n} = \dfrac{P_{xn}}{\gamma_n} \\ \dfrac{dw_{Cn}}{d\varphi_n} = \dfrac{P_{zn}}{\gamma_n} \cdot J_0(X_n) \cdot \cos\varphi_n \\ \dfrac{dw_{Sn}}{d\varphi_n} = -\dfrac{P_{zn}}{\gamma_n} \cdot J_0(X_n) \cdot \sin\varphi_n \end{cases}, \qquad (6)$$

$$\begin{cases} \varphi_{0n} = \dfrac{\pi}{2} + n \cdot \dfrac{2\pi}{N}, \qquad n = 0,..., N-1 \\ P_{zn0} = P_{xn0} = 0, \\ Z_{n0} = L_0, \\ X_{n0} = X_{\mathrm{Cathode}}, \\ w_{Sn0} = w_{Cn0} = 0. \end{cases}. \qquad (7)$$

Numerical simulation of the tracking in the median plane and disposition of the accelerating cavity relative to the axes (z, x) are shown in Fig. 1.

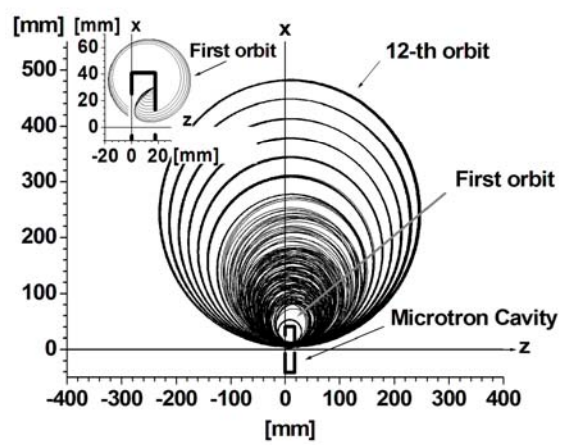

Fig. 1. 2-D tracking in median plane of the microtron. In the left corner is shown the tracking of the first orbit and the layout of the accelerating cavity having narrow radial slits for passage of the electrons.

Note that the described method allows one to consider all accelerated particles, synchronous and nonsynchronous as well, in the loading current.

Computed amplitudes of the loading current, I_C, and the accelerated current extracted from the 12-th orbit, I_{12}, (the microtron output current) as functions of the amplitude of the accelerating voltage, V_C, are plotted in Fig. 2.

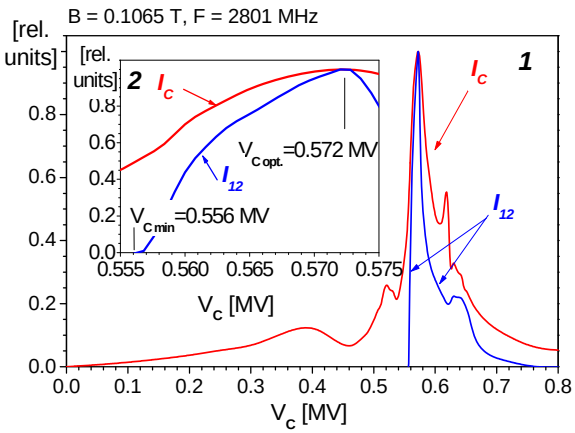

Fig. 2. Normalized amplitudes of the loading current, I_C, and the accelerated current extracted from the 12-th orbit, I_{12}, versus the accelerating voltage. In the inset, (2), the curves I_C and I_{12} are plotted in detail in the neighborhood of the microtron operating parameters.

Figure 3 shows computed phases of the loading current, φ_{I_C}, and of the extracted current from the 12-th orbit, $\varphi_{I_{12}}$, as functions of the accelerating cavity voltage. In the inset, (2), are shown detailed plots of the loading current and extracted current phases, φ_{I_C} and $\varphi_{I_{12}}$, respectively, in the neighborhood of the microtron operating conditions.

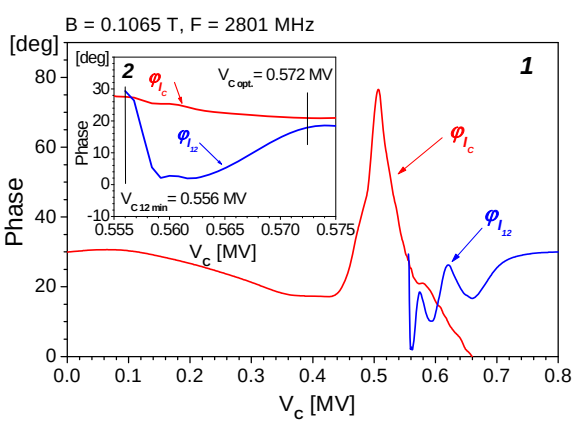

Fig. 3. Phases of the loading current, φ_{I_C}, and the extracted current, $\varphi_{I_{12}}$, as functions of the accelerating cavity voltage V_C.

The plots in Fig. 3, inset 2, show that the dependence of the phase of the loading current on V_C in the neighborhood of the microtron operating conditions is quite weak because it is a result of contributions of all bunches on all orbits and therefore it is a resulting phase averaged over all orbits; in fact this is a collective effect.

Unlike the weak dependence of the loading current phase, φ_{I_C}, on V_C, the dependence of the phase of the extracted current, $\varphi_{I_{12}}$, on V_C as shown in the inset is much stronger.

This phenomenon is caused by a transient process in the equilibrium phase establishment, it results in an additional phase instability of the extracted bunches. This causes an additional intrapulse detuning of the FEL optical resonator affecting, as it will be shown below, the FEL operation in the beginning of the macropulse.

Transient State of the Microtron Cavity and Intrapulse Stabilization of the Accelerated Current

A transient state of the microtron cavity has been computed basing on the Slowly Varying Envelope Approximation (SVEA), [8], considering loading of the cavity caused by the electron beam under acceleration. The effect of the incremental emission current caused by pulsed overheating of the emitting surface by back-streaming non-synchronous electrons, [4], was included in this consideration.

For the microtron cavity, the abridged equation for the transient state is, [8]:

$$\left\{\frac{d}{dt}+\frac{\omega_{0C}}{2Q_{LC}}\cdot\left(1-i\varepsilon_C\right)\right\}\tilde{V}_C=\frac{\omega_{0C}}{Q_{EC}}\cdot\tilde{V}_{FC}-\frac{\omega_{0C}}{2Q_{EC}\cdot Y_{0C}}\cdot\tilde{I}_C\cdot\exp\left(i\cdot\varphi_C\right) \quad (8)$$

Here $Q_{EC}=Q_{0C}/\beta_C$ and $Q_{LC}=Q_{0C}/(1+\beta_C)$ are the external and loaded cavity quality factors, respectively, Q_{0C} = 9800 (measured value) is the cavity wall quality factor, ω_{0C} is the circular eigenfrequency of the cavity, β_C = 5.4 (measured value) is the cavity coupling coefficient, $\varepsilon_C \cong -2Q_{LC}(\omega-\omega_{0C})/\omega_{0C}$ is the detuning parameter of the accelerating cavity, operating at the frequency of ω, $\tilde{V}_{FC}$ are complex amplitudes of the oscillation in the forward wave, φ_C is the phase of the complex time-dependent amplitude $\tilde{V}_C(t)$, R_{Sh} = 1.08 MOhm is the effective shunt impedance of the accelerating cavity and $Y_{0C}=2\beta_C/R_{Sh}=1.0\cdot10^{-5}$ [1/Ohm] is the external waveguide conductance of the cavity. $\tilde{I}_C$ is a complex function of $V_C(t)$. It was calculated using the dependence $\tilde{I}_C(V_C)$ plotted in Figs. 2 and 3 and equation

(5). The time-dependent normalized emission current, $i_C(t)$, and I_{0C} were obtained from measurements.

The time-domain computation of the accelerated macro-pulse current on the 12-th orbit was based on simulation of the tracking; the data were used in the equation (8) for constant magnetron power and measured incremental emission current. The result is plotted in Fig. 4, curve 1.

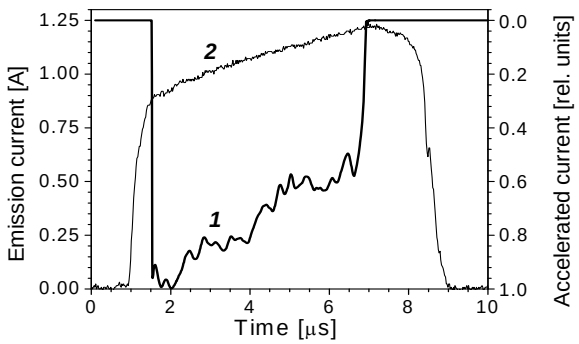

Fig. 4. Calculated shape of the accelerated current, curve 1, right scale, vs. the time-dependent measured emission current, curve 2, and left scale.

Curve 1 shows that the amplitude of the accelerated current is reduced almost by half at the end of the macro-pulse because of an increase of the emission current which causes the incremental beam loading in the accelerating cavity.

Compensation of the drop of the accelerated current was done by increasing the magnetron power during the macro-pulse by tuning the modulator charging line to provide linear increments of the magnetron current by ≈ 10%.

Fig. 5 shows the calculated shape of the accelerated current, curve 2, for the measured incremental magnetron current, curve 1. The accelerated current, curve 3, measured with an internal removable target shows satisfactory agreement between the calculations and the measurements.

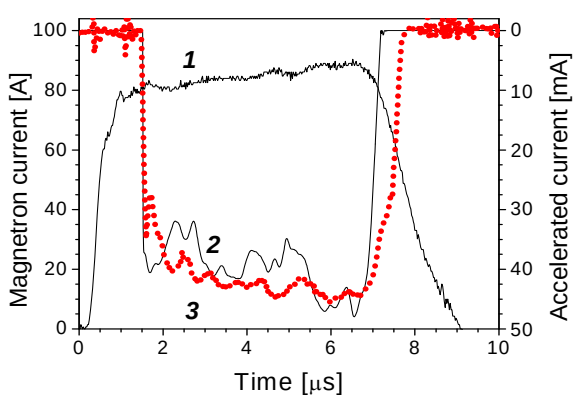

Fig. 5. Calculated, curve 2, relative units, and measured, curve 3, right scale, accelerated current at the 12-th orbit vs. the incremental magnetron current, curve 1, left scale.

Transient State of the Magnetron-Microtron Cavity System and Intrapulse Stabilization of the Magnetron Frequency

Simulation of the intrapulse instability of the magnetron frequency caused by variation of the magnetron current, and properties of the stabilizing microwave scheme employing frequency pulling in the magnetron was done using the SVEA method for the system including coupled magnetron and microtron cavities.

The abridged equation for the transient state in the magnetron cavity differs from equation (8) with the noise term only, [9]:

$$\left\{\frac{d}{dt}+\frac{\omega_{0M}}{2Q_{LM}}\cdot\left(1-i\varepsilon_M\right)\right\}\widetilde{V}_M=\frac{\omega_{0M}}{Q_{EM}}\cdot\widetilde{V}_{FM}+\frac{\omega_{0M}}{2Q_{EM}\cdot Y_{0M}}\cdot\widetilde{I}_M+\frac{\omega_{0M}}{2Q_{EM}}\cdot V_{Noise}. \quad (9)$$

Analogous to equation (8), Q_{LM} is the loaded magnetron cavity quality factor, $Q_{0M}\cong 1500$ is the wall quality factor, ω_{0M} is the circular eigenfrequency of the magnetron cavity, $\beta_M\cong 10$ is the magnetron coupling coefficient, ε_M is the detuning parameter of the magnetron cavity, operating at the frequency of ω, $\widetilde{V}_M$ and $\widetilde{V}_{FM}$ are complex amplitudes of the oscillation in the magnetron cavity and in the forward wave, respectively, $Y_{0M}=2.363\cdot 10^{-3}$ [1/Ohm] is the external waveguide conductance of the magnetron cavity, $\widetilde{I}_M$ is the complex amplitude of the first harmonic of the magnetron current, and φ_M is the phase of the complex amplitude $\widetilde{V}_M(t)$.

The noise source V_{Noise} is added in equation (9) to excite oscillations in the magnetron. It is equal, [9], to:

$$V_{Noise}(t)=\begin{cases} V_{M0}\cdot k_{Noise}\cdot\dfrac{U_A(t)}{U_{A_N}}\left[1-\dfrac{V_M(t)}{V_{M0}}\right] & \text{for } V_M(t)<V_{M0} \\ 0 & \text{for } V_M(t)\geq V_{M0}\end{cases} \quad (10)$$

Here: V_{M0}=37.7 kV is the nominal magnetron voltage,

$k_{Noise}=0.025$ is the noise coefficient,

$U_A(t)$ is the time-dependent anode voltage,

$U_{A_N}=48.98$ kV is the nominal anode voltage,

$V_M(t)=\left|\widetilde{V}_M(t)\right|$ is modulus of the magnetron cavity voltage.

More frequently for magnetrons, the concept of the electron conductance, $\widetilde{Y}_M$, is used [9]:

$$\widetilde{I}_M=\widetilde{V}_M\cdot\widetilde{Y}_M\cdot i_A(t). \quad (11)$$

Here: $i_A(t)$ is the normalized dimensionless time-dependent magnetron anode current,

$\widetilde{Y}_M = Y_{0M} \cdot y_M \cdot (1+\beta_M)/\beta_M$,

y_M is the relative electron conductance.

The relative electron conductance y_M depends on the anode voltage U_A and the modulus of the magnetron cavity voltage V_M as:

$$y_M = f(U_A) \cdot g_M(V_M) + i \cdot \sqrt{f(U_A)} \cdot b_M(V_M). \quad (12)$$

The anode function $f(U_A)$ is equal to:

$$f(U_A) = \begin{cases} 0 & \text{for} \quad U_A(t) < U_{A_T}, \\ \dfrac{U_A(t) - U_{A_T}}{U_{A_N} - U_{A_T}} & \text{for} \quad U_A(t) > U_{A_T}. \end{cases}$$

Here $U_{A_T} = 0.8 \cdot U_{A_N}$ is the threshold of the anode voltage.

The typical values of $g_M(V_M)$ and $b_M(V_M)$, the conductance and the susceptance of the magnetron cavity, respectively, were taken in accordance with [9]. Fig. 6 shows dependences of these values on the relative magnetron cavity voltage V_M / V_{M0}.

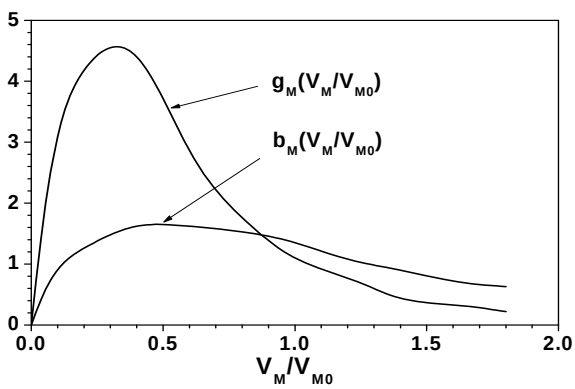

Fig. 6. Conductance, g_M, and susceptance, b_M, of the magnetron vs. relative magnetron cavity voltage, V_M / V_{M0}.

The output power of the magnetron is equal to:

$$P_{M_OUT} \equiv P_{RM} = \frac{Y_{0M}}{2} \cdot \left| \widetilde{V}_{RM} \right|^2.$$

The voltage of the reflected wave in the waveguide is:

$$\widetilde{V}_{RM} = \widetilde{V}_M - \widetilde{V}_{FM}.$$

The expression for $\widetilde{V}_{RM}$ can be presented as:

$$\widetilde{V}_{RM} = V_{RM} \cdot \exp(i \cdot \varphi_{RM}).$$

The time-dependent deviations of the magnetron frequency can be calculated from:

$$F_{RM} = \frac{1}{2\pi} \cdot \frac{d\varphi_{RM}}{dt}.$$

In Fig. 7 are shown the calculated and the measured intrapulse magnetron frequency deviations for the magnetron loaded by a passive load ($\widetilde{V}_{FM} = 0$, so $\widetilde{V}_{RM} = \widetilde{V}_M$).

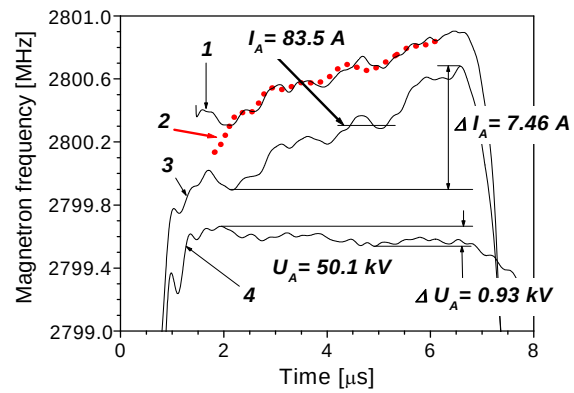

Fig. 7. Calculated, 1, and measured, 2, deviations of the frequency of the magnetron loaded by a passive waveguide load during the macropulse vs. the time-dependent magnetron current, 3.

Measured shapes of the pulse tops of the magnetron anode current and the magnetron anode voltage are plotted in curves (3) and (4), respectively.

The magnetron intrapulse frequency deviations were measured using a heterodyne method. The magnetron was loaded by the passive matched waveguide load. A directional coupler with directionality of ≈ 20 dB was used to measure the deviation of the magnetron frequency in the forward wave. The attenuated wave from the magnetron was mixed with the 2.793 GHz signal of a synthesizer and periods of the difference frequency were measured during the macro pulse with a 2 Gs/s digital oscilloscope. The measured results were averaged over 10 macro-pulses. The accuracy of the measured frequency deviations with this method is ≈ 3-5 kHz for the 100 ns time interval [10]. One can see that the magnetron frequency deviations in fact follow to deviations in the magnetron current because of the frequency pushing in the magnetron.

The simulation based on the measured time-dependent values of the magnetron pulse current and the pulse voltage shows agreement with the measured frequency deviations of the magnetron. The deviations at the incremental magnetron current are in the range of ≈ 0.8 MHz during the macro pulse in operation with a passive load.

The developed microtron-driven terahertz FEL utilizes an optical resonator with the length determined from the expression $L = 52 \cdot \frac{\lambda_b}{2} \approx 52 \cdot \frac{c}{2 \cdot f_b}$, where $\lambda_b \approx c/f_b$ is the wavelength of the accelerating voltage, and f_b is the bunch repetition rate of the accelerated current. For $f_b \approx$ 2.801 GHz, $\Delta L / \Delta f_b \approx 26(\lambda_b / f_b) \approx$ 0.99 mm/MHz, i.e., the bunch repetition rate deviations in the range of 0.8

MHz are equivalent to the FEL optical resonator detuning by ≈0.8 mm during the macro-pulse. This value is inadmissibly large for the terahertz FEL operating in the wavelength range of 0.1-0.35 mm.

To provide intrapulse stability of the bunch repetition rate acceptable for lasing in the terahertz range, we developed a simplified microwave scheme to stabilize the magnetron frequency. The scheme is based on the frequency pulling in the magnetron through the wave reflected from the accelerating cavity; in other words, the accelerating cavity serves concurrently as an external stabilizing resonator for the magnetron. The reflected wave passes through a ferrite insulator, having limited inverse loss of ≈ 18 dB at the magnetron pulse power of 1.7-2 MW. Such loss provides an acceptable level of the passing wave for the frequency pulling in the magnetron. At that the microwave microtron system was optimized in length. A layout of the microtron and the microwave system based on the MI-456A magnetron is shown in Fig. 8.

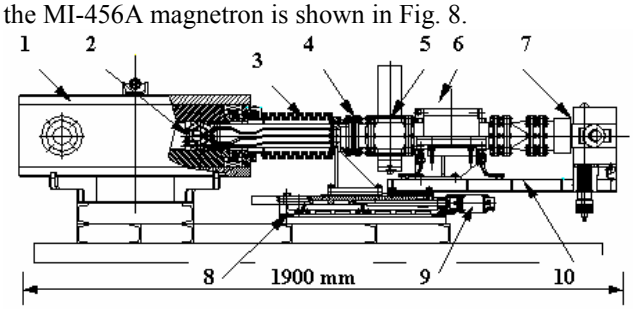

Fig. 8. Variable-energy microtron layout. 1-microtron magnet, 2-accelerating cavity, 3-long-stroke flexible bellows, 4-waveguide window, 5-waveguide directional coupler, 6-ferrite insulator, 7-magnetron, 8-moving stage, 9-moving motor, 10-movable frame.

To calculate the frequency in the coupled system of magnetron and accelerating cavities we used additional equations that considered the power relationships between the magnetron and the microtron cavities through the voltages in the reflected and forward waves in the waveguide:

$$\widetilde{V}_{RC} = \widetilde{V}_C - \widetilde{V}_{FC}\ ,\ \widetilde{V}_{RM} = \widetilde{V}_M - \widetilde{V}_{FM}\,. \qquad (13)$$

The voltages in the forward waves for the magnetron and the microtron cavities are expressed as:

$$\widetilde{V}_{FC}\cdot\sqrt{\frac{Y_{0C}}{2}} = \alpha_{M_C}\cdot\widetilde{V}_{RM}\cdot\sqrt{\frac{Y_{0M}}{2}}\,,$$

$$\widetilde{V}_{FM}\cdot\sqrt{\frac{Y_{0M}}{2}} = \alpha_{C_M}\cdot\widetilde{V}_{RC}\cdot\sqrt{\frac{Y_{0C}}{2}}\,. \qquad (14)$$

Here $\alpha_{M_C} = 0.4$ dB is the transfer coefficient from the magnetron to the microtron cavity, and $\alpha_{C_M} = 18.0$ dB is the transfer coefficient from the microtron cavity to the magnetron.

The values of $\widetilde{V}_{FC}$ and $\widetilde{V}_{FM}$ can be expressed as functions of $\widetilde{V}_C, \widetilde{V}_M$ by considering the equations (13) and (14):

$$\widetilde{V}_{FC} = \frac{\alpha_{M_C}}{1-\alpha_{M_C}\cdot\alpha_{C_M}}\left(\widetilde{V}_M\cdot\sqrt{\frac{Y_{0M}}{Y_{0C}}} - \alpha_{C_M}\cdot\widetilde{V}_C\right), \qquad (15a)$$

$$\widetilde{V}_{FM} = \frac{\alpha_{C_M}}{1-\alpha_{M_C}\cdot\alpha_{C_M}}\left(\widetilde{V}_C\cdot\sqrt{\frac{Y_{0C}}{Y_{0M}}} - \alpha_{M_C}\cdot\widetilde{V}_M\right). \qquad (15b)$$

Calculation of the frequency deviations in the coupled system of the magnetron and the microtron cavities was done using equations, (8), (9), (15a), (15b), for various detuning parameters of the microtron cavity. Note that the equations include the frequency drift in the stabilizing (accelerating) cavity caused by variation of the beam loading.

The calculated time-dependent deviations in the magnetron frequency are shown in Fig. 9 by solid lines. The solid lines with error bars are the measured magnetron frequency deviations in the coupled system. Curve 4 is the measured incremental magnetron current.

For the measurements, the magnetron was loaded by the accelerating cavity through the ferrite insulator. The frequency deviations were measured in the forward wave with the directional coupler. The measurements were done using the heterodyne method as described above at an accelerated current in the range of 42-45 mA measured on 12-th orbit, and an average emission current of ≈1.1 A.

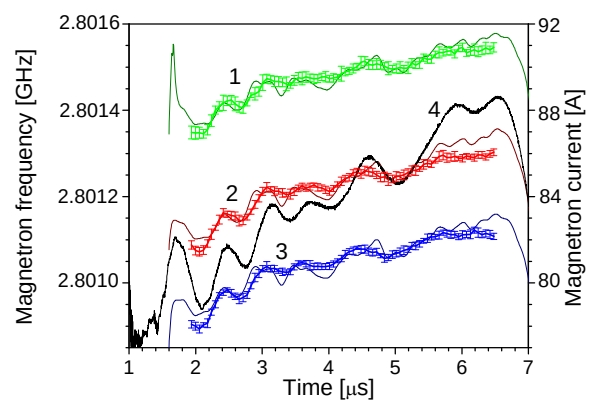

Fig. 9. Calculated (solid lines) and measured (bold solid lines with error bars) deviations of the magnetron frequency in the magnetron-accelerating cavity system, left scale, at various values of the magnetron-accelerating cavity detuning parameter, ε. 1- ε=0.47, 2- ε=0.74, 3- ε=0.93, 4- plot of the measured incremental magnetron current, right scale.

Results of the measurements and the computations, Fig. 9, are in agreement, showing the correctness of the presented computations demonstrating the intrapulse variation of the stabilized magnetron frequency in the range of 0.25 MHz with the detuning parameter ≤0.74. Comparison of the results with those presented in Fig. 7 shows that the simplified microwave scheme provides stabilization of the magnetron frequency with a coefficient of ~ 3.5.

The calculated and measured frequency oscillations in

the magnetron-accelerating cavity system, having a period of ≈0.6-0.7 μs and a relative amplitude of ≈ 10^{-5}, are in-phase with the ripple in the magnetron current, Fig. 9, curve 4, and are caused by deviations of the magnetron current during the macro-pulse with relative amplitudes of ≤1.5% (corresponding to <0.2% in the modulator pulse voltage).

Comparison of the measured drift of the magnetron frequency during the macro-pulse with the computed frequency drift of the accelerating voltage shows that the stabilizing scheme in fact suppressed the magnetron frequency drift up to the value of the frequency drift of the accelerating voltage. This drift is caused by the back-streaming electrons overheating the cathode surface resulting in incremental beam loading in the accelerating cavity, [4]. Thus it becomes necessary to minimize the emission current increment for the microtron employing internal injection and intended to drive a terahertz FEL.

Variation of the Equilibrium Phase under Transient Process in the Microtron Cavity

The amplitude and the phase of the extracted current, computed as functions of the amplitude of the accelerating voltage, allow one to compute in the time domain the deviation of the phase of the extracted current caused by variation of the equilibrium phase during the transient process.

The cavity voltage can be written in following form:

$$\widetilde{V}_C(t) = V_C(t) \cdot \exp[i \cdot \varphi_C(t)]. \qquad (16)$$

Here $V_C(t)$ is the time-dependent modulus of the cavity voltage and $\varphi_C(t)$ is the time-dependent phase of the cavity voltage. The extracted current is proportional to the time-dependent emission current, the dimensionless amplitude of the accelerated current from the 12-th orbit, depending on $V_C(t)$, and depends on the phase, $\varphi_C(t)$. The phase of the bunch at the entrance of the extracting channel depends on time as:

$$\varphi_{12}(t) = \varphi_C(t) + \varphi_{I_{12}}[V_C(t)]. \qquad (17)$$

Deviations of the frequency in the microtron accelerating cavity during the macro-pulse are computed using the following expression:

$$\Delta F_C(t) = \frac{1}{2\pi} \cdot \frac{d\varphi_C(t)}{dt}. \qquad (18)$$

It is obvious that the input microtron cavity voltage and the magnetron frequency have the same deviations.

Deviations of the bunch repetition rate caused by the phase motion of the extracted bunches are computed as:

$$\Delta F_{12}(t) = \frac{1}{2\pi} \cdot \frac{d\varphi_{12}(t)}{dt}. \qquad (19)$$

The time-dependent deviations of the repetition rate of the extracted bunches computed for the accelerating cavity detuning parameter, ε=0.74, are shown in Fig. 10 as curve C. For comparison in Fig. 10 curve B shows deviations of the accelerating frequency caused by phase deviations of the current loading the accelerating cavity during the macro-pulse. In particular, these deviations determine the stability of the frequency of the accelerating voltage in the microtron-FEL injector.

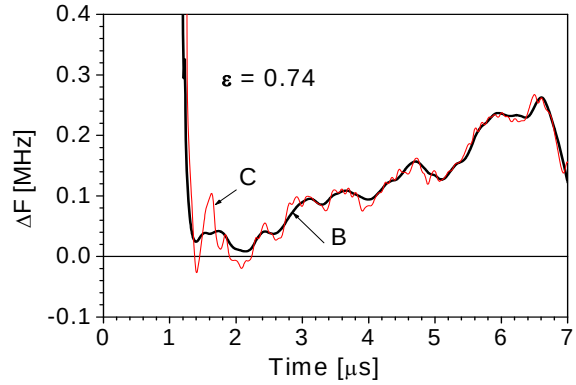

Fig. 10. B- deviations of the frequency in the microtron accelerating cavity, C- bunch repetition rate deviations of the extracted current.

Analysis of these plots shows that the average increment in both curves is approximately the same and caused by incremental loading of the accelerating cavity because of a back bombardment of the cathode surface by non-synchronous electrons. The oscillations in curve B with amplitude of ≈30 kHz, that is ≈10^{-5} of the magnetron frequency, are caused by ripples of the magnetron current because of the frequency pushing in the magnetron during the macro-pulse as was noted above. Oscillations in the bunch repetition rate, curve C, in the beginning of the macro-pulse are caused by variation of the equilibrium phase during the transient process. The effect results in an additional modulation of the repetition rate of the bunches extracted from the microtron and transported into the FEL undulator.

The establishment of the equilibrium phase is continued during the increase of the $\widetilde{V}_C$ amplitude from a minimum value, acceptable for acceleration of the electrons over all orbits in the microtron and corresponding to 0.556 MV, to the optimum operating value, corresponding to ≤0.572 MV, as is shown in Fig. 3, inset 2.

Optimization of the Magnetron-Driven Microtron-Injector of the Terahertz FEL

Regimes of the magnetron-driven microtron-injector employing intrapulse stabilization of the accelerated current and the magnetron frequency have been optimized for maximum macro-pulse lasing energy to user applications.

The optimization at a given accelerated current included minimization of the microtron cathode current to decrease

the magnetron frequency deviation. The minimization prolongs the cathode life time that is also important for users.

Consideration of the beam dynamics shows that the range of variation of the equilibrium phase has a strong dependence on the detuning parameter when the accelerating cavity is well matched with the loading beam. An increase of the detuning parameter increases the amplitude of the equilibrium phase deviation that increases the amplitude of the frequency modulation of the extracted bunches. The effect has been studied by measuring the intrapulse bunch repetition rate deviations at various values of the detuning parameter.

To measure the intrapulse bunch repetition rate, the electron beam extracted from the 12-th orbit was transported through a low Q-factor measuring cavity integrated into a beam line, [10]. The cavity signal containing information about the bunch repetition rate has been measured using a heterodyne method in the manner described above. The microtron parameters were optimized to provide a macro pulse current of 40-42 mA in the beam line at a minimized increment of the emission current and an average emission current of ≈1.1 A. The modulator charging system provided constant charging voltage with accuracy better than 0.1%.

Results of these measurements for various detuning parameter values are shown in Fig. 11 by bold solid lines with error bars. The detuning parameter was varied by mechanical tuning of the magnetron. For comparison in this figure, the measured intrapulse magnetron frequency deviations are plotted by dots with the same color.

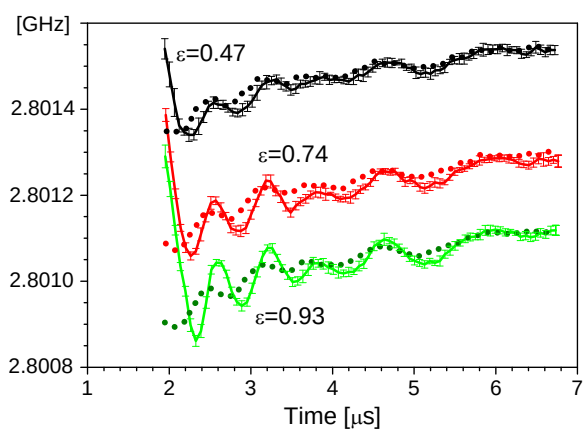

Fig. 11. Measured deviations in the bunch repetition rate (bold solid lines with error bars) and the magnetron frequency (dots) for various values of the detuning parameter, ε.

The plotted curves show that the measured deviations of the magnetron frequency, with a period of ~0.6 μs and an amplitude of ~30 kHz, are in fact similar in shape for all considered values of the detuning parameter. However the measured repetition rate of the extracted bunches in the first half of the accelerated macropulse current demonstrates an additional oscillation noticeably different from deviations of the magnetron frequency. The amplitude of the oscillation strongly depends on the detuning parameter, as was noted above, in agreement with the beam dynamic consideration.

The additional bunch repetition rate oscillation does not affect the microtron operation in the considered range of accelerated current; however it affects the FEL operation, in fact causing an additional intrapulse detuning of the FEL optical resonator. The phenomenon was studied in operation of the terahertz FEL, [11]. For that we have measured the terahertz FEL power signal varying the detuning parameter.

During the measurements the modulator charging voltage was kept constant. The accelerated current also was kept constant with accuracy better than 3.5% to keep a constant current at the entrance of the FEL undulator. The accelerated beam injected into the FEL undulator was extracted from the 12-th orbit of the microtron and the FEL was tuned for lasing at λ=110 μm. The microtron operating parameters were optimized to get minimal increments of the emission current at the accelerated macro-pulse current of 42 mA. The lasing macro-pulse power was measured by a wideband Schottky-barrier detector, [12].

Fig. 12 (a) shows the measured lasing pulse shapes for various values of the magnetron-accelerating cavity detuning parameter.

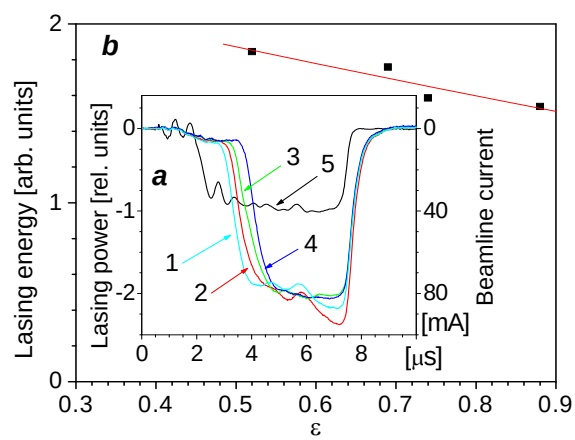

Fig. 12. a) Variation of the lasing macro-pulse shape vs. the magnetron-accelerating cavity detuning (left scale). 1- ε=0.52, 2- ε=0.69, 3- ε=0.74, 4- ε=0.88, 5- shape of the beamline current. b) Variation of the lasing macro-pulse energy at a wavelength of 110 μm vs. the detuning parameter.

Plot b in Fig. 12 shows the measured drop of the lasing energy with an increase of the detuning parameter. The drop is a result of the additional frequency modulation in the bunch repetition rate that is caused by variation of the equilibrium phase during the transient process.

The plots in the inset (a) show a noticeable growth of the buildup time with an increase of the detuning parameter. Since the last one determines the value of the maximum accelerated current, the microtron parameters have to be

optimized for minimum detuning in the system magnetron-accelerating cavity at a given accelerated current injected into the FEL. In this case, one can provide maximum energy in lasing and maximum lasing macropulse duration.

Optimizing the microtron parameters and minimizing the detuning parameter, we provided operation of the microtron-driven terahertz FEL with a measured extracted macropulse lasing energy of ≈ 0.2 mJ at a macropulse power of 40-50 W in the range of 1.5-3 THz. The measured rms deviation in the lasing macropulse energy was less than 9% for long-time (few hours) measurements, [4].

Summary

A compact and inexpensive high-current magnetron-driven classical microtron has been developed as an injector of the widely tuneable terahertz FEL. Computations based on 2D tracking and transient process simulation have been done to calculate in the time domain the microtron accelerated current, deviations of the frequency of the accelerating voltage, and deviations of the repetition rate of the bunches feeding the FEL. The calculations validate simple in realization concepts and techniques for the intrapulse stabilization of the accelerated current and the bunch repetition rate in the microtron-FEL injector. The realized concepts allowed the development of the laboratory-sized, inexpensive, and reliable terahertz FEL. The effect of the equilibrium phase variation during the transient process has been studied through computations and experiments that allowed optimization of the microtron-FEL injector operation. Long-time operation of the facility demonstrated that the microtron provides operation of the FEL in the range of 1-3 THz with extracted lasing power of 30-50 W in the macropulse having durations of 2.5-4 μs. The standard deviations of the lasing macro-pulse energy are less than 9% for long-term operation. The widely tunable terahertz FEL based on the magnetron-driven classical microtron-injector has demonstrated stable and reliable operation for users for more than 5 years.

Acknowledgement

We are very thankful to Dr. R. Thurman-Keup for fruitful discussions.

References

[1] G.M. Kazakevitch, S.O. Cho, Y.U. Jeong, B.C Lee, J. Lee, V.P. Belov, N.G. Gavrilov, in Proceed. of the PAC 2001 Conference, edited by P. Lucas and S. Weber, V.4, 2739-2741, IEEE, New York, 2001,

[2] Y.U. Jeong, G.M. Kazakevitch, B.C. Lee, S.O. Cho, J. Yoo, N.G. Gavrilov, V.V. Kubarev. NIM A 507 (2003), 125-128.

[3] S.P. Kapitza and V.N. Melekhin, in The Microtron, edited by E.M. Rowe (London, Harwood Academic Publishers, 1978), Vol. 1, p. 6-12.

[4] G.M. Kazakevich, V.M. Pavlov, G.I. Kuznetsov, Y.U. Jeong, S.H. Park and B.C. Lee, JOURNAL OF APPLIED PHYSICS, 102, 034507 (2007)

[5] G.Kazakevitch, Y.U Jeong, V.M. Pavlov, B.C. Lee, NIM A 528, (2004), 115-119

[6] L.B. Lugansky, and V.N. Melekhin, in "High power electronics", Nauka, Moscow, 1965, pp. 238-256, (in Russian).

[7] Atsuko Takafuji et al., Numerical Analysis of electron Orbits in a Compact High-Current Circular Microtron. IEEE Trans on Nucl. Science, V44, 4, 1677-1683,1997

[8] D.H. Whittum, Frontiers in accelerator technology, U.S.-CERN-Japan International School, Japan, edited by S.I. Kurokawa, M. Month, and S. Turner (World Scientific, Singapore, London, 1996), pp. 1-135.

[9] V.N. Zavorotilo, O.S. Milovanov, Accelerators, V. 16, (Atomizdat., Moscow, 1977), pp. 34-37, (In Russian).

[10] G.M. Kazakevitch, Y.U. Jeong, B.C. Lee and J. Lee. NIM A 483 (2002), 331-335.

[11] G.M. Kazakevitch, Y.U. Jeong, B.C. Lee, N.G. Gavrilov, M.N. Kondaurov, NIM A 507, (2003), 146-149.

[12] V.V. Kubarev, G.M. Kazakevich, Y.U. Jeong, and B.C. Lee. NIM A 507 (2003), 523-526.